



POLITECNICO
MILANO 1863

ATTITUDE PROJECT

Giulia Sala
10582449

Academic year 2020/2021
MSc in Space Engineering
School of Industrial and Information Engineering
Course of Spacecraft Attitude Dynamics

Abstract

The aim of this report is to design and discuss the ADCS of a satellite in a Low Earth Orbit. The SIMULINK logic which has been followed will be presented through the blocks which have been implemented, all the decisions and hypotheses taken will be explained and justified in details. The behaviour of the attitude of the satellite has been studied during two different modes: the Free Control mode and the Controlled mode.

During the first one the satellite is in a Free Tumbling mode and it is possible to show how it reacts to the disturbances coming from the external environment.

Instead the second mode is characterized by the active role of the Attitude Control and it is divided into two different phases. The DeTumbling phase which starts from the release of the satellite from the launcher and ends when the satellite is sufficiently slowed down in order to be able to reach the second phase. This one is the Earth Pointing phase in which the spacecraft has reached the desired angular velocity and configuration pointing the LVLH reference frame.

Nomenclature

Symbol	Unit of Measure	Description
I	[kg/m^2]	Inertia matrix
h_p	[km]	Perigee altitude
h_a	[km]	Apogee altitude
e	[$-$]	Eccentricity
i	[$^\circ$]	Inclination
ω	[$^\circ$]	Anomaly of the perigee
Ω	[$^\circ$]	RAAN
R, R_E	[km]	Earth radius
G	[Nm^2/kg]	Constant of universal gravitation
m_t	[kg]	Earth mass
V_b	[$-$]	Vector in the body reference frame
V_n	[$-$]	Vector in the inertial reference frame
r	[km]	Distance of the satellite from Earth
S	[km]	Distance of Sun from Earth
ADCS		Attitude Determination and Control Subsystem
ARW		Angular Random Walk
RRW		Rate Random Walk
LEO		Low Earth Orbit
SRP		Solar Radiation Pressure
ERRP		Earth Reflected Radiation Pressure
ERP		Earth Radiation Pressure

Contents

1	Introduction	1
1.1	Satellite	1
1.2	Orbit Definition	1
2	SIMULINK Model Overview	2
2.1	Dynamics	2
2.2	Kinematics	3
2.2.1	Direction Cosines	3
2.2.2	Quaternions	3
2.3	Perturbations	3
2.3.1	Gravity Gradient	4
2.3.2	Solar Radiation Pressure	4
2.3.3	Atmospheric Drag	5
2.3.4	Magnetic Field	5
3	Attitude Determination	6
3.1	Sensors	6
3.1.1	Sun sensor	6
3.1.2	Magnetometer	7
3.1.3	Earth Horizon	7
3.1.4	Gyroscope	7
3.2	Determination Algorithms	8
3.2.1	QUEST-method	8
3.2.2	Analytic solution to Wabha's problem	9
3.3	Filtering	9
3.3.1	Linear Observer	9
4	Attitude Control	10
4.1	DeTumbling	10
4.1.1	Non linear control	10
4.2	Earth pointing	11
4.2.1	Linear control	11
4.3	Actuators	11
4.3.1	Magnetorquers	11
4.3.2	Reaction Wheels	12

5	Results	12
5.1	Kinematics	12
5.2	Perturbations	13
5.3	Attitude determination	15
5.4	Control Free motion	16
5.5	Controlled motion	16
5.5.1	Angular velocity and Attitude	16
5.5.2	Sensors Accuracy	17
5.5.3	Actuators	18
6	Conclusions	19
7	References	20

1 Introduction

1.1 Satellite

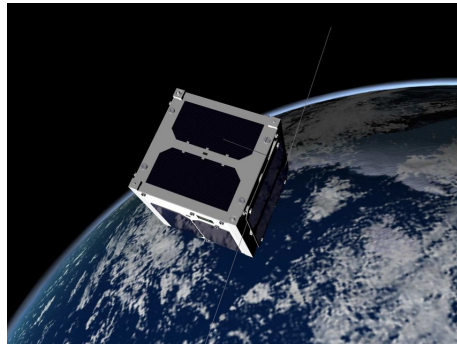


Figure 1: AAUSAT-II Satellite

The satellite which will be presented in this report is inspired by the AAUSAT-II by Aalborg University and in the table below the satellite characteristics, including sensors and actuators are reported:

Table 1: AAUSAT-II Characteristics

Mass [kg]	Dimensions [m]	Sensors	Actuators
1	0.1×0.1×0.1	Sun sensor Magnetometer Earth Horizon sensor Gyroscope	3 Magnetorquers 1 Reaction Wheel

The values of the principal inertia axes of the designed spacecraft are the following:

$$I = \begin{bmatrix} 0.0014 & 0 & 0 \\ 0 & 0.0015 & 0 \\ 0 & 0 & 0.0017 \end{bmatrix} [kg \cdot m^2] \quad (1)$$

1.2 Orbit Definition

The orbit in which the satellite has been injected is a Sun-synchronous near-circular one having the following orbital elements:

Table 2: Keplerian elements of the orbit

h_p [km]	h_a [km]	e [-]	i [$^\circ$]	ω [$^\circ$]	Ω [$^\circ$]
574	589	0.0011	97.5	317.4	48.5

2 SIMULINK Model Overview

In this first chapter different blocks implemented in the SIMULINK simulation will be presented.

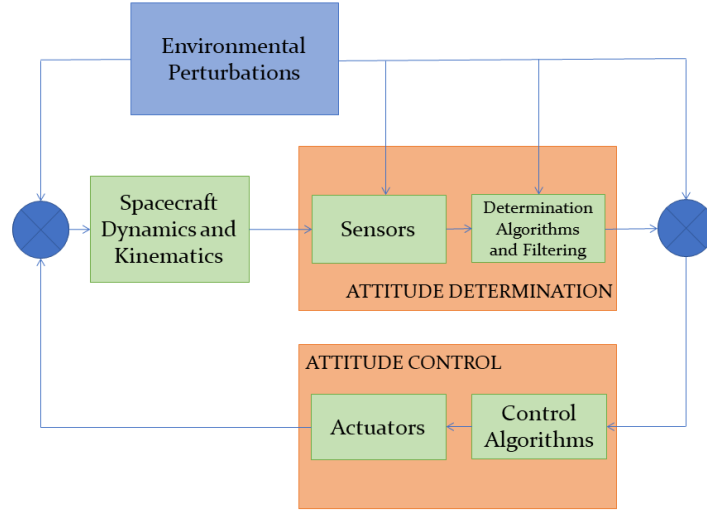


Figure 2: Block scheme implemented in SIMULINK

2.1 Dynamics

In this first block the dynamics of the satellite in the body reference frame is described by the Euler Equations which have been written referring to the principal inertia axes 1. Here it is shown how the components of the total torque M caused by the environmental perturbations and the effective control torque given by actuators directly change the components of the angular velocity w .

$$\begin{cases} \dot{w}_x = \frac{I_y - I_z}{I_x} w_y w_z + \frac{M_x}{I_x} \\ \dot{w}_y = \frac{I_z - I_x}{I_y} w_x w_z + \frac{M_y}{I_y} \\ \dot{w}_z = \frac{I_x - I_y}{I_z} w_x w_y + \frac{M_z}{I_z} \end{cases} \quad (2)$$

Since the Euler equations are a set of differential equations in order to compute the angular velocity an initial integrating value is required. This value has been considered as the angular velocity with which the satellite is released by the launcher.

Table 3: Angular velocities at the release

Yaw [°]	Pitch [°]	Row [°]
0.2	0.2	0.25

2.2 Kinematics

The angular velocity integrated by the Dynamics block enters the Kinematics one in which the attitude parameters have been calculated. These show the time development of the angular position of the spacecraft expressed in its own body reference frame with respect to the LVLH reference frame. Direction cosines (project requirements) have been implemented to find out the satellite kinematics.

2.2.1 Direction Cosines

The attitude matrix expressed with direction cosines:

$$\frac{dA_{B/N}(t)}{dt} = -[w \wedge] A_{B/N}(t) \quad [w \wedge] = \begin{bmatrix} 0 & -w_z & -w_y \\ w_z & 0 & -w_x \\ -w_y & w_x & 0 \end{bmatrix} \quad (3)$$

The matrix has been orthonormalized at each time step as described below in order to preserve its structure.

$$A_{B/N}(t) = \frac{3}{2} A_{B/N_0}(t) - \frac{1}{2} A_{B/N_0}(t) A_{B/N_0}^T(t) A_{B/N_0}(t) \quad (4)$$

2.2.2 Quaternions

In order to do a comparison also the kinetics through quaternions has been performed.

$$\frac{dq(t)}{dt} = \frac{1}{2} \Omega q(t) \quad \Omega = \begin{bmatrix} 0 & w_z & -w_y & w_x \\ w_z & 0 & w_x & w_y \\ w_y & -w_x & 0 & w_z \\ -w_x & -w_y & -w_z & 0 \end{bmatrix} \quad (5)$$

The structure of quaternions has to be preserved. Once quaternions have been computed they have been normalized at each time step and then the attitude matrix has been written through quaternions as follow:

$$A_{B/N} = (q_4^2 - \underline{q}^T \underline{q}) I + 2\underline{q}\underline{q}^T - 2q_4[\underline{q} \wedge] \quad (6)$$

2.3 Perturbations

Now the disturbing torques acting on the satellite and so affecting its attitude motion will be analyzed.

2.3.1 Gravity Gradient

The gravity gradient torque results from a non uniform gravity field over the spacecraft and it is strongly correlated with its shape. The mathematical model for the aforementioned torque follows:

$$\begin{cases} M_x = \frac{3Gm_t}{R^3} \frac{(I_z - I_y)}{I_x} c_3 c_2 \\ M_y = \frac{3Gm_t}{R^3} \frac{(I_x - I_z)}{I_y} c_1 c_3 \\ M_z = \frac{3Gm_t}{R^3} \frac{(I_y - I_x)}{I_z} c_2 c_1 \end{cases} \quad (7)$$

The torque depends on the attitude of the satellite which is represented by the direction cosines c_i and they are obtained as follows:

$$\begin{bmatrix} c1 \\ c2 \\ c3 \end{bmatrix} = A_{B/L} \begin{bmatrix} 1 \\ 0 \\ 0 \end{bmatrix} \quad (8)$$

where $A_{B/L}$ is the rotation matrix from the LVLH to the body reference frame.

2.3.2 Solar Radiation Pressure

Since the satellite is orbiting at an altitude between 500 and 600 km all the three different sources of the electromagnetic radiation have been taken into account. As a matter of fact at the orbit's altitude the radiation reflected by the Earth and the Earth radiation play an important role from the disturbance point of view.

Direct solar radiation The solar radiation when hits the outer surfaces of the satellite generates a pressure which turns into a force and a torque around the centre of the satellite mass. In mathematical terms the torque is given by:

$$T_{SRP} = \sum_{i=1}^n \vec{r}_i \times [-P_{SRP} A_i (\hat{S}_b \cdot \hat{N}_{bi}) [(1-\rho_s) \hat{S}_b + (2\rho_s (\hat{S}_b \cdot \hat{N}_{bi}) + \frac{2}{3}\rho_d) \hat{N}_{bi}]] \quad \hat{S}_b \cdot \hat{N}_{bi} > 0 \quad P_{SRP} = \frac{Fe_{SRP}}{c} \quad (9)$$

Radiation reflected by the Earth The radiation reflected by the Earth torque results from the reflection of the solar radiation given by the Earth as follows:

$$T_{ERRP} = \sum_{i=1}^n \vec{r}_i \times [-P_{ERRP} A_i (\hat{S}_b \cdot \hat{N}_{bi}) [(1-\rho_s) \hat{S}_b + (2\rho_s (\hat{S}_b \cdot \hat{N}_{bi}) + \frac{2}{3}\rho_d) \hat{N}_{bi}]] \quad \hat{S}_b \cdot \hat{N}_{bi} > 0 \quad P_{ERRP} = \frac{Fe_{ERRP}}{c} \quad (10)$$

Eclipse condition The torque of the direct radiation from the Sun and the one reflected by the Earth are equal to zero when the satellite is in the eclipse phase. In order to represent this event the following eclipse condition has been implemented in the two mathematical models:

$$\mathbf{r}_n \cdot \hat{\mathbf{S}}_n < -\sqrt{|\mathbf{r}_n|^2 - R_E^2} \quad (11)$$

Earth radiation The last contribution which has been taken into account is the torque resulting from the radiation generated by the Earth:

$$T_{ERP} = \sum_{i=1}^n \vec{r}_i \times [-P_{ERP} A_i (\hat{\mathbf{S}}_b \cdot \hat{\mathbf{N}}_{bi}) [(1-\rho_s) \hat{\mathbf{S}}_b + (2\rho_s (\hat{\mathbf{S}}_b \cdot \hat{\mathbf{N}}_{bi}) + \frac{2}{3}\rho_d) \hat{\mathbf{N}}_{bi}]] \quad \hat{\mathbf{r}}_b \cdot \hat{\mathbf{N}}_{bi} > 0 \quad P_{ERP} = \frac{Fe_{ERP}}{c} \quad (12)$$

2.3.3 Atmospheric Drag

When the satellite interacts with the upper atmosphere it has to face with aerodynamics forces which generate a torque about the centre of mass of the spacecraft. The atmospheric drag torque is not negligible for orbits below 700 km of altitude and can be modeled as follows:

$$T_{aero} = -\frac{1}{2} \rho C_d v_{rel}^2 \sum_{i=1}^n \vec{r}_i \times \frac{\vec{v}_{rel}^b}{|v_{rel}^b|} \sum_{i=1}^n (\hat{\mathbf{N}}_{Bi} \frac{\vec{v}_{rel}^b}{|v_{rel}^b|}) A_i \quad \hat{\mathbf{N}}_{Bi} \frac{\vec{v}_{rel}^b}{|v_{rel}^b|} > 0 \quad C_d = 2.1 \quad (13)$$

v_{rel} is the relative velocity between the satellite and the atmosphere:

$$v_{rel} = V_{s/c} - w_e \times R_{s/c} \quad (14)$$

ρ is the air density and it depends on the orbit altitude:

$$\rho(h) = \rho_{ref} e^{\frac{h-h_0}{H_{ref}}} \quad (15)$$

2.3.4 Magnetic Field

The magnetic field can be considered similar to a dipole field only above 7000 km from ground so at the current altitude the Earth's magnetic field has to be modeled. In particular it has been patterned as the gradient of a scalar potential where V is the potential function, normally expressed as a series expansion of spherical harmonics:

$$V(r, \theta, \phi) = R \sum_{n=1}^k \left(\frac{R}{r}\right)^{n+1} \sum_{m=0}^n (g_n^M \cos(m\phi) + h_n^m \sin(m\phi)) P_n^m(\theta) \quad (16)$$

Where r, θ, ϕ are the spherical coordinates of the position of the satellite.

Explicitly we have:

$$B_r = -\frac{\partial V}{\partial r} \quad B_\theta = -\frac{1}{r} \frac{\partial V}{\partial \theta} \quad B_\phi = -\frac{1}{r \sin \theta} \frac{\partial V}{\partial \phi} \quad (17)$$

The coefficients g_n^m and h_n^m are subjected to time variation and they refer to the IGRF.

3 Attitude Determination

3.1 Sensors

The selected sensors which are necessary to the attitude determination of the satellite will be presented in this section. They are not the real sensors equipped on AAUSAT-II but they have been conscientiously chosen accordingly to the environment in which the satellite moves.

The sensors have been implemented taking into account the following two equations which represent the results that come out from a real sensor:

$$\hat{b}_b = A_\epsilon A_{B/N} \hat{b}_n \quad (18)$$

The above equation takes as inputs the following matrix, $A_{B/N}$ which is the rotation matrix from the inertial to the body reference frame and the normalized vector in the inertial frame and gives as output the measurements of the sensor in its body reference frame which coincides with the body reference frame of the satellite.

$$A_\epsilon = \begin{bmatrix} \cos \psi \cos \theta & \cos \psi \sin \theta \sin \phi + \sin \psi \cos \phi & -\cos \psi \sin \theta \cos \phi + \sin \psi \sin \phi \\ -\sin \psi \cos \theta & -\sin \psi \sin \theta \sin \phi + \cos \psi \cos \phi & \sin \psi \sin \theta \cos \phi + \cos \psi \sin \phi \\ \sin \theta & -\cos \theta \sin \phi & \cos \theta \cos \phi \end{bmatrix} \quad (19)$$

Where ψ, θ, ϕ are generated by the Random Number Generator block provided by SIMULINK in which the variance has been selected according to the accuracy of each sensor. So the A_ϵ matrix represents the random noise contribution in sensors measurements due to the internal construction of sensors themselves.

3.1.1 Sun sensor

The Sun sensor block is modeled in order to take as input the normalized vector expressing the Sun position in the inertial reference frame and to give as output the same vector in the body frame as shown in 18 The selected Sun sensor is NanoSSOC-A60 by Solar MEMS which has the following specifics:

Table 4: NanoSSOC-A60 by Solar MEMS

Field of view	$\pm 60^\circ$
Accuracy	$< 0.5^\circ$
Precision	$< 0.1^\circ$
Dimensions	$43 \times 14 \times 5.9$ mm
Mass	6.5 g
Power supply	5 V

3.1.2 Magnetometer

The magnetometer measures the direction of the Earth's magnetic field in the sensor reference frame. This has been implemented in the magnetometer block as shown in 18. The selected magnetometer is NMRM-001-485 by NewSpace which has the following specifics:

Table 5: NMRM-001-485 by NewSpace

Orthogonality	$< \pm 1^\circ$
Dimensions	$69 \times 45 \times 20$ mm
Mass	67 g
Power supply	5 V

3.1.3 Earth Horizon

The Earth Horizon is able to detect the horizon of the Earth and to reconstruct from this its relative position. The Earth Horizon block takes as input the normalized vector expressing the Earth position in the inertial reference frame and gives as output the same vector in the body frame of the satellite through 18. The selected Earth Horizon is CubeIR by CubeSpace which has the following specifics:

Table 6: CubeIR by CubeSpace

Field of view	$120 \times 90^\circ$
Accuracy	$< 1.5^\circ$
Dimensions	$26 \times 26 \times 30$ mm
Mass	50 g
Power supply	3.3 V

3.1.4 Gyroscope

The satellite's angular velocity measured by the gyroscope has been expressed as shown in the following and has been integrated through the gyroscope dynamics.

$$w_i^{mes} = w_i + n + b \quad (20)$$

The values n , b represent two different types of errors which indicate the white noise effecting the gyroscope's measurements. Each of these two values is function of ξ ; a random value generated by the Random Number Generator block provided by SIMULINK in which the variance has been assumed unitary and a parameter directly coming from the specific of the chosen gyro:

$$n = \sigma_n \xi_n \quad b = \sigma_b \xi_b \quad (21)$$

$$\sigma_n = \frac{ARW}{\sqrt{T_s}} \quad RRW = \frac{B_i}{\sqrt{T_s}} \quad \sigma_b = \frac{RRW}{\sqrt{T_s}} \quad (22)$$

T_s is the sampling time and ARW , RRW are directly correlated to the selected STIM202 ButterfliesGyro by SensoNOR specifics:

Table 7: STIM202 ButterfliesGyro by SensoNOR

Bias Instability	0.4°/hr
ARW	0.17°/hr ^{0.5}
Sample rate	1000 samples/s
Sample frequency	262 Hz
Dimensions	38.6×35.9×20 mm
Mass	55 g
Power supply	5 V

3.2 Determination Algorithms

The attitude determination has been modeled following the QUEST-method but a comparison has been done with the Analytic solution to Wabha's problem. They are both statistical methods through which can be obtained a better estimation of the attitude matrix $A_{B/N}$. Both of these two methods to determine the $A_{B/N}$ matrix need at least two vector measurements and the knowledge of the relative precision of the sensors α_i . During the sunlight the attitude determination is provided thanks to three sensors: Sun, Earth and magnetic field sensor. Instead during the eclipse phase the Sun sensor is no longer available and so only the other two sensors are used.

3.2.1 QUEST-method

This first method intends to reconstruct the $A_{B/N}$ matrix computed through quaternions. Since the QUEST-method is based on the fact that measurements are not perfect before the conversion to quaternions the following weighted error function has to be minimized:

$$J(A) = 1 - \sum_{i=1}^N \alpha_i (s_{bi}^T A_{B/N} \nu_i) = 1 - \sum_{i=1}^N q^T K q \quad (23)$$

Which is equal to maximize:

$$\tilde{J} = q^T K q \quad q^T q = 1 \quad (24)$$

$$K = \begin{bmatrix} S - \sigma I & Z \\ Z^T & \sigma \end{bmatrix} \quad (25)$$

$$B = \sum_{i=1}^N \alpha_i s_{bi} v_{ni}^T \quad (26)$$

$$S = B + B^T \quad (27)$$

$$Z = [B_{23} - B_{32}, \quad B_{31} - B_{13}, \quad B_{12} - B_{21}]^T \quad (28)$$

$$\sigma = \text{tr}[B] \quad (29)$$

The structure of quaternions has to be preserved. Once quaternions have been computed they have been normalized at each time step and then the rotation matrix can be reconstruct as 6.

3.2.2 Analytic solution to Wabha's problem

Similarly to the previous method the following weighted error function has to be minimize:

$$J(A) = \frac{1}{2} \sum_{i=1}^N \alpha_i |s_{bi} - A_{B/N} \nu_i|^2 \quad (30)$$

Which means to maximize:

$$\tilde{J}(A) = \sum_{i=1}^N \alpha_i s_{bi}^T A_{B/N} \nu_i = \text{tr}(A_{B/N} B^T) \quad A_{B/N} = (B^T)^{-1} (B^T B) = B(B^T B)^{-1/2} \quad (31)$$

Where B is computed through 26.

3.3 Filtering

A specific filtering procedure has been implemented in order to attenuate the noise naturally coming from the sensors measurements. Following this procedure more clear signals have been obtained. A low pass filter has been the first choice but then it has been replaced by a Linear Observer. This because the Linear Observer doesn't introduce any phase loss instead of the low pass filter and also because it's not trivial to find a suitable cut off frequency for the filter.

3.3.1 Linear Observer

The filtering procedure adopted to reduce the white noise of the gyro effecting its angular velocity estimation is the following:

$$\begin{cases} \dot{w}_x^{est} = \frac{I_y - I_z}{I_x} w_y^{est} w_z^{est} + \frac{M_x}{I_x} + l(w_x^{est} - w_x^{mes}) \\ \dot{w}_y^{est} = \frac{I_z - I_x}{I_y} w_x^{est} w_z^{est} + \frac{M_y}{I_y} + l(w_y^{est} - w_y^{mes}) \\ \dot{w}_z^{est} = \frac{I_x - I_y}{I_z} w_x^{est} w_y^{est} + \frac{M_z}{I_z} + l(w_z^{est} - w_z^{mes}) \end{cases} \quad (32)$$

It is based on the integration of the new dynamics. It has as inputs the components of the angular velocity directly measured by the gyro w_i^{mes} and of the new estimated one w_i^{est} , the components of the total torque M_i which is the sum of the total torque from the disturbs and the total effective torques from actuators and the gain l . This last one shapes the magnitude of the last term as well as the transient for the optimal tracking.

Instead the filtering action to reduce the noise coming from Sun sensor, Earth Horizon and Magnetometer has been patterned as follow:

$$\dot{A_{B/N}^{est}} = -[w^{mes} \wedge] A_{B/N}^{est} + l(A_{B/N}^{est} - A_{B/N}^{sens}) \quad (33)$$

It results from the integration of the new estimated kinematics and it takes as inputs the new estimated kinematics and the one measured by sensors and the w_i^{mes} from the gyro.

4 Attitude Control

In this chapter will be presented how the Controlled Mode has been designed in terms of control logic and actuators. This mode is characterized by the active role of the actuators and it is divided into two different phases: the DeTumbling and the Earth Pointing phase in which the satellite reaches the desired angular velocity and attitude.

4.1 DeTumbling

The DeTumbling phase begins after the deployment of the spacecraft and during this manoeuvre the angular velocity along the roll, pitch and yaw axes of the satellite have to be slowed down. In particular the initial value at the beginning of the DeTumbling phase has been considered as the release velocity from the launcher 3. The DeTumbling phase has been considered accomplished and concluded once the components of the angular velocity has reached a value around 0.0021 rad/s. After this phase the satellite is ready to perform the pointing manoeuvre which will be explained in the following section.

4.1.1 Non linear control

Only one particular value of the initial angular velocity has been taken into account but in general this mission phase is characterized by a wide range of initial angular velocities depending on the launcher selection. For this reason a non linear control has been implemented. The non linear control theory is based on the Lyapunov's second stability theorem and can be used to prove global stability to the system. The kinetic energy can be used as a candidate Lyapunov function to determine suitable controls and substituting it in the dynamics equation the results is the following:

$$Mc = -Kb_{DET} w_{B/L_{error}} \quad (34)$$

$$\begin{cases} A_{B/L_{error}} = A_{B/N_{error}} A_{L/N_{error}}^T \\ w_{B/L_{error}} = w_{B/N_{mes}} - A_{B/L_{error}} w_{L/N} \end{cases} \quad (35)$$

$$w_{L/N} = [0; 0; n] \quad n = \sqrt{\frac{\mu}{a^3}} \quad (36)$$

$-Kb_{DET}$ is a tuning parameter, $A_{B/L_{error}}$ and $w_{B/L_{error}}$ are the matrix and angular velocity attitude error respectively.

4.2 Earth pointing

This second phase starts some seconds after the DeTumbling one when the angular velocity has been reduced and the aim of the Earth Pointing is to satisfy the pointing requirement of the satellite towards the Earth.

4.2.1 Linear control

The Earth Pointing phase has been satisfied through the implementation of a linear control and this is justified by the fact that the angular velocity are very small thanks to the previous phase. In order to accomplished the Earth Pointing two are the targets which have to be reached: the angular velocity $w_{L/N}$ 36 and $A_{L/N}$ which is the rotation matrix from the inertial to the LVLH reference frame. A PD controller has been implemented as follow in order to provide the required control action:

$$\begin{cases} Mc_x = -\frac{1}{2}Kp_{EP}(a_{23} - a_{32}) - Kd_{EP}w_{B/L_{error_x}} \\ Mc_y = -\frac{1}{2}Kp_{EP}(a_{31} - a_{13}) - Kd_{EP}w_{B/L_{error_y}} \\ Mc_z = -\frac{1}{2}Kp_{EP}(a_{12} - a_{21}) - Kd_{EP}w_{B/L_{error_z}} \end{cases} \quad (37)$$

It takes as inputs the components of the matrix and angular velocity attitude error 35 and the two tuning parameters Kp_{EP} and Kd_{EP} .

4.3 Actuators

For both the first and the second phase of the Controlled Mode three magnetotorquers and one reaction wheel has been used as actuators. Each magnetotorquers has been aligned with the satellite body axes and the reaction wheel has been placed along the pitch direction.

4.3.1 Magnetotorquers

Magnetotorquers generate a torque by inducing a magnetic dipole in a coil which is surrounded by the Earth's magnetic field:

$$Mc = \underline{D} \wedge \underline{B} \quad \underline{D} = \mu n S \underline{I} \quad (38)$$

The specifics of the three magnetotorquers chosen are reported below:

Table 8: MT01 Compact Magnetorquer by EXA

Nominal Magnetic Moment	>0.19 Am ²
Saturation Magnetic Moment	>0.85 Am ²
Dimensions	50×50×4.3 mm
Mass	7.5 g
Power supply	from 250 mW to 1750 mW

4.3.2 Reaction Wheels

Reaction wheels are actuators based on acceleration and deceleration of spinning rotors which have a nominal condition of zero angular velocity. The presence of a wheel allows the matrix of the configuration to be non singular and it is also used for redundancy. The chosen reaction wheel is the CubeWheel small by Cube Space:

Table 9: CubeWheel small by Cube Space

Momentum Storage @8000 rpm	1.7 mNms
Dimensions	28×28×26.1 mm
Mass	60 g

It is very small since the quasi total amount of the control torque given by actuators is provided by the three magnetorquers.

5 Results

All the results will be shown along one orbital period except for the Free Control Mode.

5.1 Kinematics

As it is reported below the error between the two different methods has an order of 10^{-3} which can be considered as a negligible value:

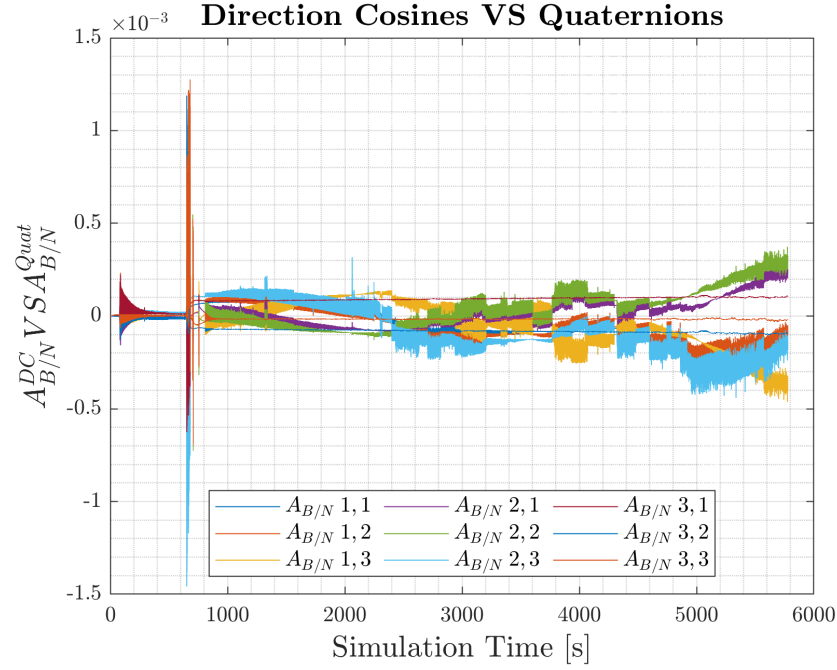


Figure 3: Error between the two kinematics methods

5.2 Perturbations

Comparisons between each perturbation in the Uncontrolled Mode and in the Controlled Mode are reported in the following. Since the satellite has a high spinning rate during the uncontrolled motion all the perturbations have a fast rate of change. Instead during the controlled motion the rate of change of the disturbances slowed down thanks to the activation of the actuators which allow the satellite to reach a low angular velocity.

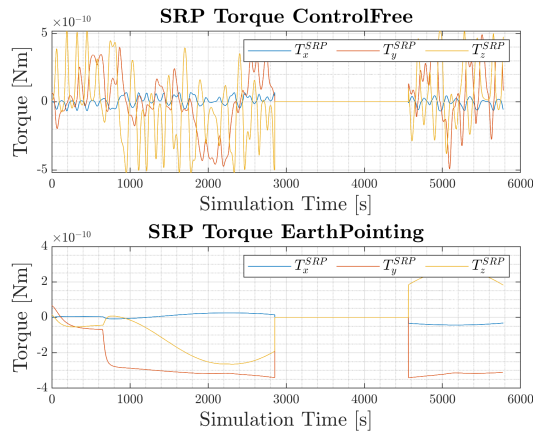


Figure 4: SRP Torque

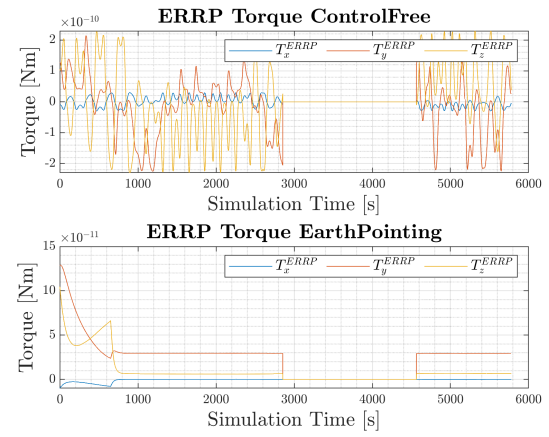


Figure 5: EERP Torque

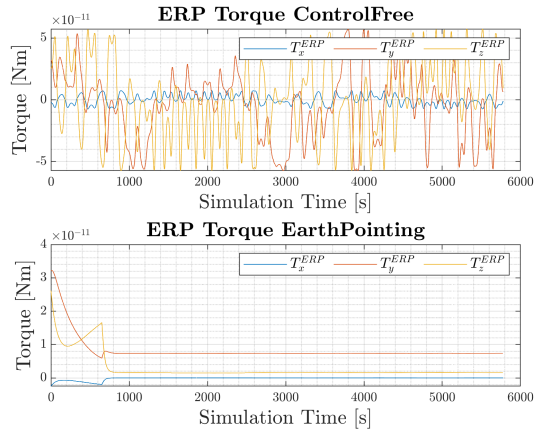


Figure 6: ERP Torque

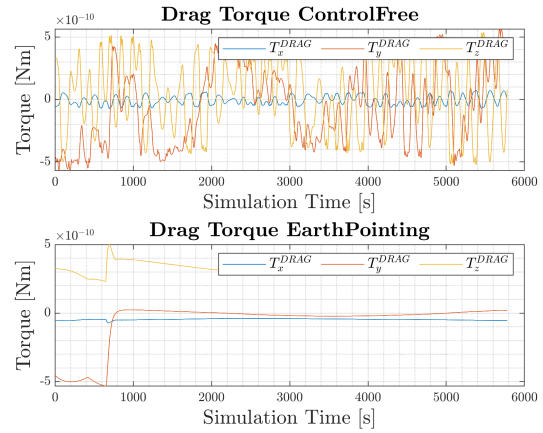


Figure 7: Aerodynamic Drag Torque

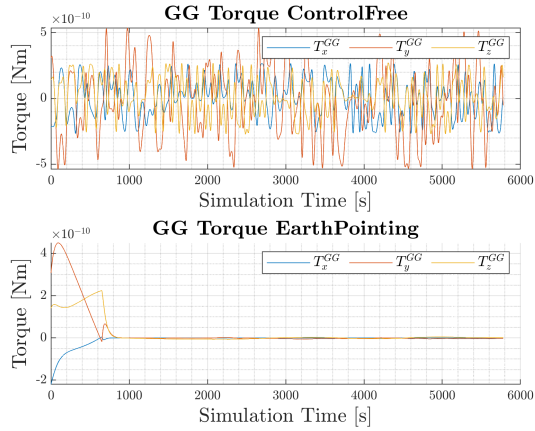


Figure 8: Gravity Gradient Torque

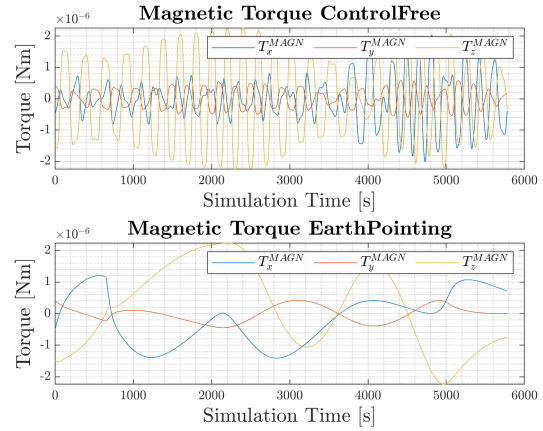


Figure 9: Magnetic Field Torque

SRP Torque The direct solar radiation pressure goes with the inverse of the square distance between the satellite and the Sun so it is almost constant for geocentric orbit because the distance to the Sun doesn't change significantly and this can be seen in the Figure 4.

ERRP and ERP Torque Instead the other two radiations are strongly dependent on the orbit radius. Since during the orbit the satellite has almost the same distance from the Earth the constant pattern of torques from the Earth reflected radiation pressure 5 and the Earth radiation pressure 6 are quite constant along all the directions.

Aerodynamics Drag Torque Regarding the torque deriving from the aerodynamic drag 7 it has a relevant importance among all the other disturbs since it plays a significant role in LEO orbits. Even though the variation between the orbit altitude at the perigee and at the apogee is

very small this effects the pattern of the torque from the aerodynamic drag and due to the change of density.

Gravity Gradient Torque During the Controlled Mode the disturb caused by the gravity gradient 8 decreases reaching almost zero. This because during the pointing phase the $A_{B/L}$ matrix becomes the identity one and the disturb is only sensitive to oscillations around this last one.

Magnetic Field Torque The torque caused by the Earth's magnetic field 9 is the most significant which is acting on the satellite. Its repetitive pattern is due to the presence of peaks which occur when the spacecraft passes above the magnetic poles.

5.3 Attitude determination

As it is reported below the error between the two different attitude determination algorithms has a order of 10^{-15} so it's an negligible value:

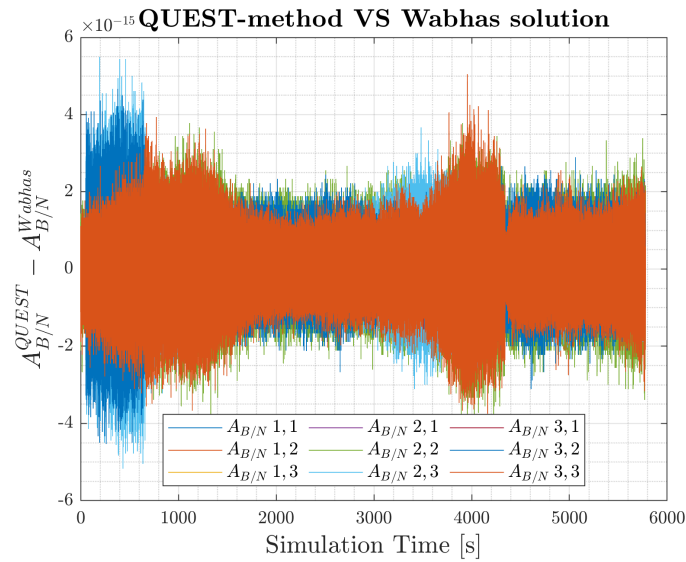


Figure 10: Error between the two attitude algorithms

5.4 Control Free motion

The uncontrolled components of the angular velocity during five orbital periods don't diverge to higher value than 3 degree/s so their behaviour is a stable one as shown in Figure 11. Since the satellite is a 1U CubeSat with low inertial components and they have almost all the same value the behaviour of the angular velocity is a peculiar one. In particular the angular velocity behaviour is driven by the total torque provided by the disturbs which is equivalent to torque of the magnetic field since all the torques from the other disturbs are smaller as shown in Figure 12.

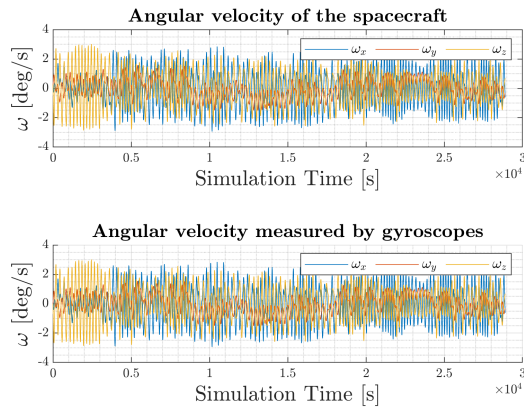


Figure 11: Angular velocity

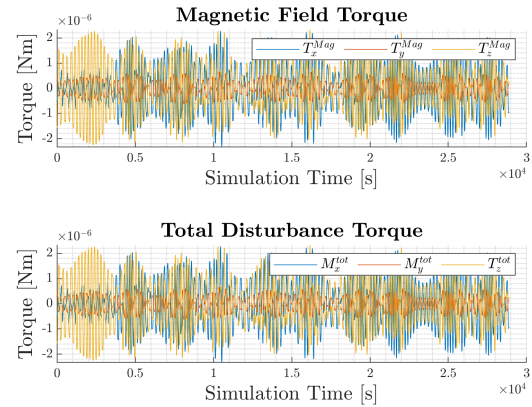


Figure 12: Magnetic VS Total torque

5.5 Controlled motion

5.5.1 Angular velocity and Attitude

The Figures 13 and 14 show the attitude parameters during the Controlled Mode. From these two figures the DeTumbling and the Earth Pointing phase are easily recognizable. Until $T=650$ s the satellite is in the DeTumbling phase so its angular velocity is strongly slowed down in order to have a value under 0.0021 rad/s but the spacecraft is not pointing during this phase. This first phase is needed because of the high angular rate with which the satellite can be released. As a matter of fact over 1 degree/s structural problems can occur and cause failure. After the DeTumbling the angular velocity is maintained equal to the desired value 36 and the satellite starts the pointing phase. The body reference frame of the spacecraft results to be aligned to the LVLH one with a good pointing error 15. In order to have a reference value of this last one it has been calculated as $\text{tr}(I - A_{B/L_{\text{error}}})$ where I here is the identity matrix and it results having an order of magnitude around 10^{-4} . Finally what can be noticed is the fact that the first peaks present in the controlled angular velocity are caused by the change in the control logic adopted and the other are due to the peaks in the magnetic field torque.

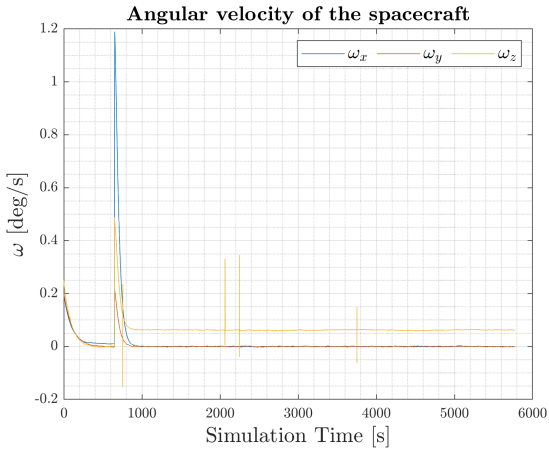


Figure 13: Angular velocity

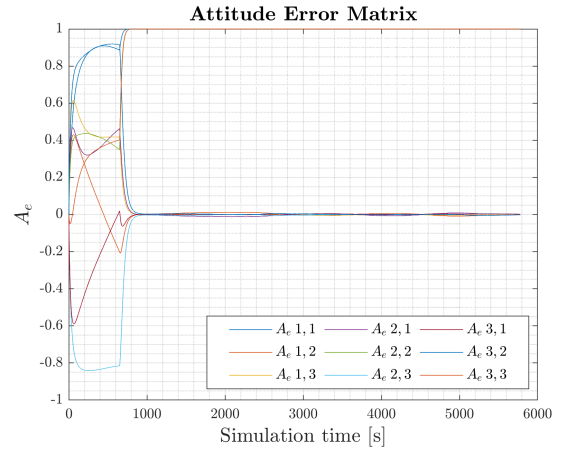


Figure 14: Attitude Error Matrix

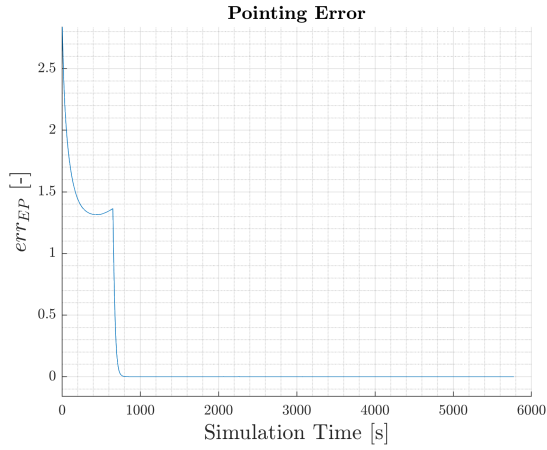


Figure 15: Pointing Error

5.5.2 Sensors Accuracy

The errors committed by the gyroscope during the measurement of the dynamics of the satellite in Figure 16 and the one coming from sensors in the attitude determination are reported in this section. The errors are both of the order of 10^{-3} and they strongly depend on the linear observer gain. Since the satellite chosen is very small in a first attempt the gyroscope was used to determine the attitude during the eclipse phase in order to not involve the Horizon sensor. Afterwards this idea was discarded because the error affecting the attitude determination was too high.

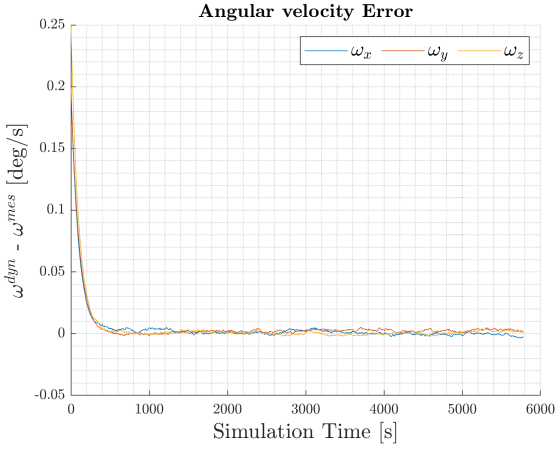


Figure 16: Angular velocity Error

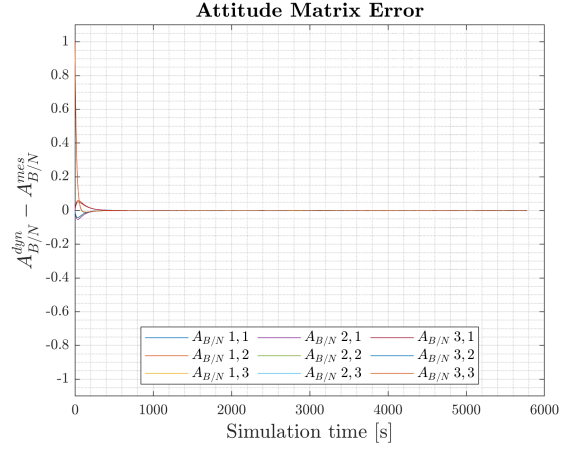


Figure 17: $A_{B/N}$ Matrix Error

5.5.3 Actuators

As is shown in Figure 19 the actuators capable of giving the effective control torque which is required in order to counteract the total torque coming from the environmental perturbations (in Figure 18) are three magnetometers aligned as the body axes and one reaction wheel along the pitch direction. Different configurations have been tried before ended up with the current solution which allows to have small peaks in the angular velocity (in Figure 13) and a high pointing accuracy. Putting the wheel along the pitch axes is also justified by the fact that it is one of the most disturbed axes. Some of the peaks in the effective torque are present in order to neutralize the ones in the total disturbance torque corresponding to the peaks in the torque provided by the magnetic field while the others occur at the change of the control logic.

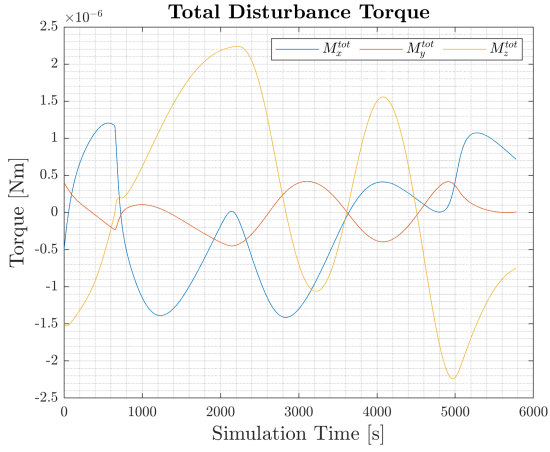


Figure 18: Total Disturbance Torque

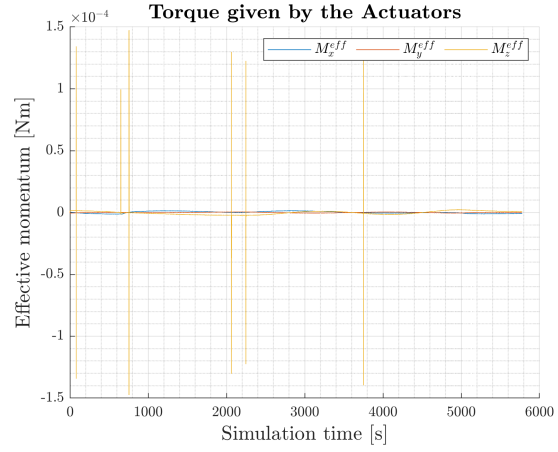


Figure 19: Effective Torque

Actuators saturation In this final section the magnetorquers (Figure 20) and reaction wheel saturation (Figure 21) are reported. Both of the two saturation limits have been imposed by the

datasheet of the actuators as shown in Table 9 and in Table 8. The actuators during the peaks of the effective torque reach values around the critical ones and then desaturate.

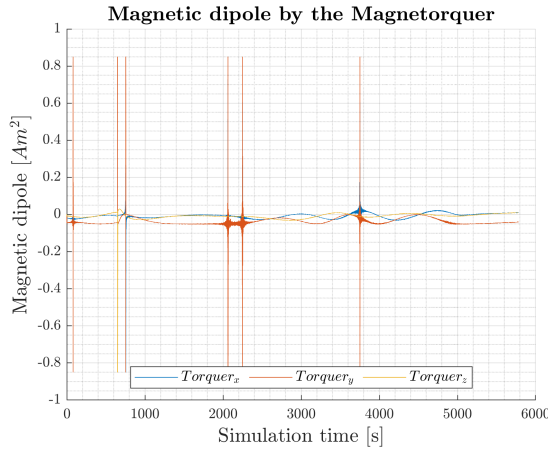


Figure 20: Magnetorquer Saturation

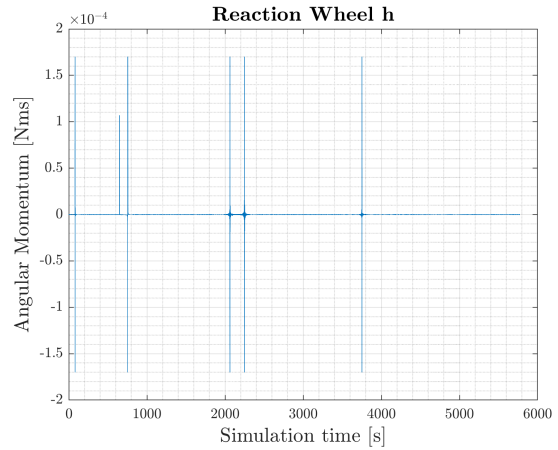


Figure 21: Reaction Wheel Saturation

6 Conclusions

The reached pointing performance is a good one since the body reference frame results to be aligned to the LVLH one with an error minor than 1 degree. This has been obtained thanks to the linear control logic implemented for the Earth Pointing phase and thanks to the gain inserted in the Linear Observer. Furthermore the optimal pointing condition has been reached quickly and right after the change of the control logic from the non linear to the linear one and the already mentioned pointing error has been maintained during the whole orbit. The time spent to reach the desired final velocity during the DeTumbling phase is also a rational and satisfying one. The actuators are capable of providing the ideal torque required by the control logic. The only drawback is the fact that the magnetorquers and the reaction wheel work near the saturation values and this could be a problem in the attitude control system. Anyway this event has been inevitable considering the actuators chosen and the good results obtained in terms of peaks in the controlled angular velocity and the pointing accuracy which all have been reached in a relative small time.

7 References

- [1] AAUSat-2 - eoPortal (<https://directory.eoportal.org/web/eoportal/satellite-missions/a/aausat-2>)
- [2] Franco Bernelli, *Spacecraft Attitude Dynamics and Control*. Politecnico di Milano, 2020
- [3] *Falcon 9 Launch Vehicle User's Guide*. SpaceX, 2009
- [4] James D. Biggs, *Spacecraft Attitude Dynamic*. Politecnico di Milano, 2020
- [5] B.O.Andresen et al. *Attitude Control System for AAUSAT-II*. Aalborg University, 2005
- [6] Jeremy Davis. *Mathematical modeling of Earth's Magnetic Field*. Virginia Tech, 2004